

Collapsing method for detailed recognition of seismogenic structures activated during underground mining.

Andrzej Leśniak¹, Elżbieta Śledź¹, and Katarzyna Mirek¹

¹AGH University of Science and Technology

November 23, 2022

Abstract

In rock mass disturbed by mining activity, distortions in the stress balance may lead to seismic energy being emitted in rejuvenated seismogenic structures. One way of increasing the imaging resolution of these seismically active structures is through relocation, which itself can be achieved using the cloud collapsing method. This method partially eliminates perturbations in the location of seismic energy sources concerning the actual positions of these sources. It enables phenomena to be grouped into spatially ordered structures that can correspond to actual tectonic structures, such as fractures, fissures or faults. The article presents results of applying the collapsing method in mining seismology using cloud of tremors recorded during mining activity at one of the coalfaces in the Bobrek hard coal mine. The relocation procedure was applied to all the foci of tremors recorded during mining activity on face 3/503 between 04.2009 and 07.2010. In the relocated point cloud two types of linear structure responsible for generating tremors are distinguished: structures directly related to mining activity and structures associated with local tectonics. The location of the separated structures of the first type corresponds to the range of coalface 3/503 and the shafts delimiting earlier mined seams 507 and 509 located below. The isolated structures of the second type, with almost vertical orientation, are associated with existing zones of discontinuity that become seismically active as a result of mining activity. The identified structures lie near the biggest tremors recorded, which is evidence that these structures may correspond to real discontinuity zones.

10 **Abstract**

11 In rock mass disturbed by mining activity, distortions in the stress balance may lead to seismic
12 energy being emitted in rejuvenated seismogenic structures. One way of increasing the imaging
13 resolution of these seismically active structures is through relocation, which itself can be
14 achieved using the cloud collapsing method. This method partially eliminates perturbations in
15 the location of seismic energy sources concerning the actual positions of these sources. It enables
16 phenomena to be grouped into spatially ordered structures that can correspond to actual tectonic
17 structures, such as fractures, fissures or faults. The article presents results of applying the
18 collapsing method in mining seismology using cloud of tremors recorded during mining activity
19 at one of the coalfaces in the Bobrek hard coal mine. The relocation procedure was applied to all
20 the foci of tremors recorded during mining activity on face 3/503 between 04.2009 and 07.2010.
21 In the relocated point cloud two types of linear structure responsible for generating tremors are
22 distinguished: structures directly related to mining activity and structures associated with local
23 tectonics. The location of the separated structures of the first type corresponds to the range of
24 coalface 3/503 and the shafts delimiting earlier mined seams 507 and 509 located below. The
25 isolated structures of the second type, with almost vertical orientation, are associated with
26 existing zones of discontinuity that become seismically active as a result of mining activity. The
27 identified structures lie near the biggest tremors recorded, which is evidence that these structures
28 may correspond to real discontinuity zones.

29 **1 Introduction**

30 Underground mining of mineral resources (e.g. hard coal) or energy resources (e.g. crude oil,
31 natural gas or geothermal energy) leads to changes in stress distribution in mining areas. These
32 changes can disturb the stress balance and trigger dynamic phenomena in the form of seismic
33 tremors of varying degrees of energy.

34 In the case of underground hard coal mining, a number of studies have noted the bimodal
35 distribution of seismic energy (Gibowicz and Kijko, 1994; McGarr, 2000; Stec, 2007) which in
36 general indicates two types of seismic phenomena associated with mining. The first type includes
37 low and medium energy seismic tremors, which most often occur in the immediate vicinity of
38 longwall faces or exploited chambers, usually as a result of mining activity. A characteristic
39 feature of the mechanism behind these phenomena is the high share of non-shear components.
40 The second type comprises medium and high energy phenomena associated with the renewal of
41 old fractures and faults. They assume the form of tremors whose mechanisms are dominated by
42 shear components. Their location is closely connected with the position of renewed seismogenic
43 structures and may be located at a greater distance from coalfaces than the first type of
44 phenomenon.

45 In many underground mines, including the Bobrek hard coal mine in southern Poland that is
46 described in the article below, both categories of seismic events occur. Numerous phenomena
47 directly induced by the fracturing of the rock mass occur in areas of mining activity and in the
48 case of this mine are concentrated above the mind coal seam or directly below it. The sources of
49 the second group of phenomena recorded during the course of mining activity are located
50 significantly (over 500 m) below the exploited coal seam. Due to the mechanism of their sources,
51 these phenomena are mainly associated with a fault network whose existence is postulated based

52 on tectonic and structural studies as well as on the genesis of individual geological structures.
53 Their existence and location can only be inferred indirectly from seismic emissions.
54 The article attempts to determine the structures responsible for the generation of seismic
55 phenomena in the Bobrek mine. For this purpose, the authors employed a method that involved
56 collapsing a cloud of seismic sources in seam 503 as well as isolating active microtectonic
57 structures (e.g. fissures and fractures) located in this area. The collapse is performed in the
58 direction of local density centers of a cloud of seismic sources to increase the latter's resolution
59 to map the structures responsible for the generation of seismic phenomena (Jones and Stewart,
60 1997). As the research shows, this method allows phenomena to be grouped into more spatially
61 ordered structures such as lines or planes. These may correspond to actual tectonic structures
62 such as fractures, fissures or faults.

63 First, the author will discuss the geological structure in the Bytom Basin area in which the
64 Bobrek Coal Mine is located, together with the structural and geomechanical factors that
65 contribute to high seismic activity both in this and in neighbouring areas. This will be followed
66 by a description of the collapsing method applied to the seismic sources along with an example
67 illustrating its effectiveness. Due to the significant impact that seismic emission location errors
68 have on the collapsing procedure, the authors also addressed the problem of identifying errors in
69 the location of emission sources recorded during the advance of the coalface. In the next part of
70 the article, the author presents data recorded during the mining of seam 503 as well as the results
71 of their relocation following the application of the collapsing procedure. Based on the above the
72 next section identifies structures with a simple, linear geometry that is responsible for generating
73 some of the tremors. These results were then set against the earlier results of seismicity studies in
74 this area. In the discussion concluding the final chapter, the author presents the benefits of the
75 analyzed method in studies of mining-induced seismicity, as well as their limitations.

76 **2 Geological structure and seismicity in the area covered by the study**

77 The occurrence of mining tremors depends on many factors, including the geological and
78 tectonic structure, the location of the coalface, and past exploitation. The interaction of these
79 factors has a significant impact on the formation of tremors.

80 The Bytom Basin forms a wide trough along a W-E axis and constitutes part of the Paleozoic
81 Variscan structure which has been cut up by numerous faults. The Bytom Basin is an
82 asymmetrical and relatively shallow trough with a complex structure. Its axis runs latitudinally
83 from West to East near the north-eastern flank. As a consequence, the layers in this flank have
84 quite steep angles of collapse which range from 8 to 20 degrees, while in the southern flank they
85 do not exceed 3 degrees. The complex structure of the basin is additionally disturbed by a
86 network of faults, mainly running in NW-SE direction and perpendicular to them, the planes of
87 which have different projections and angles of inclination. Large faults with throw values of
88 between several meters and almost 300 meters are accompanied by a network of smaller faults
89 with throw values ranging in size from several dozen centimeters up to approximately 20 m.

90 Carboniferous formations in the studied area reach a thickness of up to 550 m and contain
91 numerous coal seams of varying thickness, up to a maximum of 12 m. A characteristic feature of
92 the carboniferous period is its cyclical structure expressed by the alternating occurrence of
93 sandstone, silt, claystone, conglomerates, and coal. These rocks differ in terms of their elastic
94 properties and compressive strength. For example, sandstone has higher strength parameters than
95 claystone and coal. One additional factor that has a decisive impact on the geomechanical
96 properties of rocks is tectonics in all its forms (faults, joints, cleavage, and other
97 inhomogeneities), which significantly reduces the strength of the rock massif.

98 In the past, the Bytom Basin had been an area of very intensive hard coal mining. In the 1990s
99 production was scaled back significantly and exploitation of zinc-lead ore was brought to an end,
100 as a result of which the rate of subsidence decreased together with the number of high-energy
101 tremors. However, this is still an area where mining activity continues to have a negative impact
102 on the surface and continues to generate seismic tremors.

103 The propensity for rock bursts to occur in a rock mass depends on the geomechanical properties
104 of the rock. It was found, for example, that an area was particularly susceptible to tremors when
105 thick benches of strong rock, such as sandstone or mudstone are located in the vicinity of a
106 deposit(Goszcz, 1999). Another influential factor is old tectonic stresses occurring in the rock,
107 which have led to changes in geomechanical properties, increasing or decreasing their propensity
108 for rock bursts.

109 In the Upper Silesian Coal Basin, tremors caused by coal mining activity are concentrated in
110 several areas, one of which is the Bytom Basin. The susceptibility of a rock mass to rock bursts
111 is explained in different ways. Studies have revealed a close relationship between mining activity
112 and low energy tremors, while more powerful tremors are associated with the tectonics of the
113 Upper Silesian Coal Basin. The widespread occurrence of rock bursts in the Bytom Basin was
114 initially explained as being the result of increased stresses in the syncline folds. However, it
115 seems that the higher risk of rock bursts in these basins is due to the compaction of rocks,
116 whereas in the past all three principal tectonic stresses were compressive in character(Goszcz,
117 1999).

118 Stec proposed a general classification of the seismic tremors in this area, which involved
119 dividing them into three groups(Stec, 2007, 2009).The first group consists of tremors with a
120 slipping and shearing foci mechanism. Tremors of this type occur during progressive mining as a
121 result of fractures in the seam of thick and compact rock complexes with high rigidity and
122 strength parameters. The second group consists of tremors characterized by foci with a non-
123 shearing mechanism. Such tremors are located directly in the coal seam and in the vicinity of
124 active coalfaces. The third group comprises "regional" tremors, characterized by the highest
125 energy, which usually occur far from areas of active mining activity. Their foci have a slip
126 mechanism that is normal or reversible in character. The most common cause of these events is
127 the interaction of tectonic and residual stresses existing in the analyzed area with mining-induced
128 stresses.

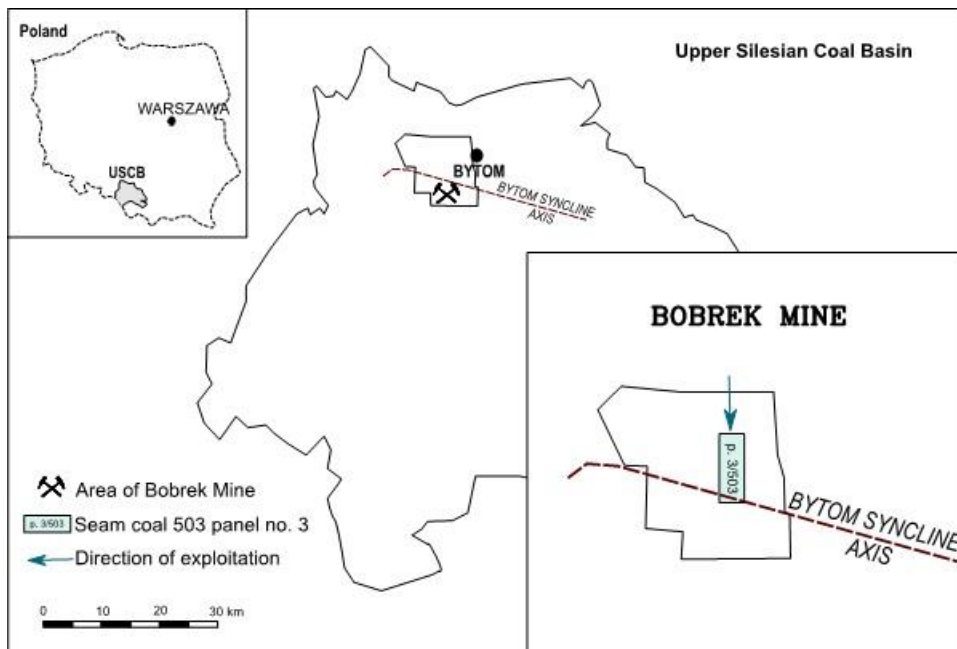
129 The exploitation area of the Bobrek mine encompasses the region of the Bytom Basin (see
130 Figure 1). This is one of the three areas where the majority of mining tremors were recorded,

131 including high energy tremors with magnitudes of up to 4.0. During the mining of face 3 in seam
 132 503 (3/503), the first tremors were observed in April 2009. The area remained seismically active
 133 until July 8, 2010. Most of the recorded tremors were low energy tremors. However, four higher
 134 magnitude tremors were also registered: 2.9 (20.05.2009), 3.7 (16.12.2009), 3.0 (5.02.2010) and
 135 2.8 (11.03.2010).

136 Marcak and Mutke (2013) analyzed tremors recorded by mining seismological stations during
 137 mining of coalface 3/503. The authors concluded that tectonic stresses were of key importance in
 138 the distribution of seismic tremors. It was also observed that higher energy tremors began to
 139 occur as the coalface reached the axis of the Bytom Basin. The hypocentres of high energy
 140 tremors were located at a depth of 300 m to 800 m below the mined seam. At the same time, it
 141 was noted that once they had passed through the Bytom Basin the energy produced by these
 142 tremors weakened and the depth of their hypocentres also decreased. The latter still occurred
 143 below the mined seam, but at a depth of less than 200 m. Furthermore, the authors showed that
 144 high-energy tremors occurring in the vicinity of the Bytom Basin had a different character to the
 145 phenomena typical of the Upper Silesian Coal Basin. The mechanism of these phenomena is
 146 associated with slipping in reverse faults, and the nature of the phenomena indicates a
 147 relationship between them and tectonics.

148 These results were partially confirmed in the work of Kozłowska et al.(2016). In this article, the
 149 authors analyzed a 3.7 magnitude tremor that occurred on December 16, 2009, during the course
 150 of mining coalface 3/503. The tremor mechanism indicates a reverse fault with an almost vertical
 151 plane. Numerical models that took into account current and past mining activity indicate that the
 152 phenomenon is associated with tectonics. However, mining activity affected a change in the
 153 stresses present in the local tectonics, which in turn triggered a fault process or the formation of a
 154 new fault on the weakening plane.

155



156

157 **Figure 1.** Location of the Bobrek mine area against the background of the Upper Silesian Coal
158 Basin.

159 **3 Theory**

160 To ensure more precise imaging of seismically active microtectonic structures based on
161 registered seismic emissions, the authors proposed applying the collapsing method(Fehler et al.,
162 1997; Jones and Stewart, 1997; Phillips et al., 1997). This is one of the techniques used to help
163 identify the microtectonic structures responsible for the emission of some of the tremors
164 accompanying the stimulation and exploitation of hydrothermal reservoirs and hydrocarbon
165 deposits.

166 The collapsing method differs from other methods employed to locate seismic sources in the way
167 it uses information regarding errors in the location of hypocenters of seismic events. Classical
168 approaches, such as the P-time method(Geiger, 1912), or techniques that take into account not
169 only the arrival times but also the direction of seismic rays(Leśniak, 2015) minimize the
170 functional describing the differences between the measured times and/or directions and their
171 values calculated based on the assumed velocity model. For minimization purposes, it is the
172 linear version of this functional that is most often performed. In this case, a location error is
173 represented as an error ellipsoid(Havskov and Ottemoller, 2010. Its spatial orientation depends
174 on the relative location of the emission source and sensors, and the volume illustrates the level of
175 confidence with which the emission source is found inside the ellipsoid. The spatial distribution
176 of a location error only assumed the form of an ellipsoid if the minimized functional is
177 linearised. When other methods are employed to determine the minimum functional (e.g. the
178 Monte Carlo simulation methods, for example in the MCMC variant(Mosegaard and Sambridge,
179 2002)), location error distributions are often not ellipsoidal in shape(Leśniak and Pszczoła,
180 2008). They depend to a great extent, on both the configuration of the sensor network and the
181 quality of registration as well as on the specific location method used(Rudziński and Dębski,
182 2013).

183 In the case of the source collapsing method, the location error is used not only to determine the
184 location accuracy of a particular emission source but also to determine the course of the
185 relocation of emission sources. The relocation (referred to in the collapsing method described
186 below) of sources takes place within the boundaries of the error ellipsoid, and thus the new
187 distribution of the sources (following the collapsing process) may reflect the actual spatial
188 distribution of the foci of tremors undisturbed by the location error. This distribution is usually
189 characterized by greater regularity and less spatial dispersion(Jones and Stewart, 1997). There
190 are several variations of the original collapsing method. Asanuma et al. proposed a modification
191 of the first version of the collapsing method, where structure of the cloud depends on the
192 distribution of locations within confidence ellipsoid(Asanuma et al., 2001). Additionally, in the
193 modified collapsing procedure location movements depend on the dimensionality on the
194 estimated original structures. In other publications, Asanuma et al. presented (Asanuma et al.,
195 2005, 2008) another modification of the collapsing method that uses mutual coherency of
196 waveforms and to establish the similarity of events. Here in the paper we use the original
197 collapsing method.

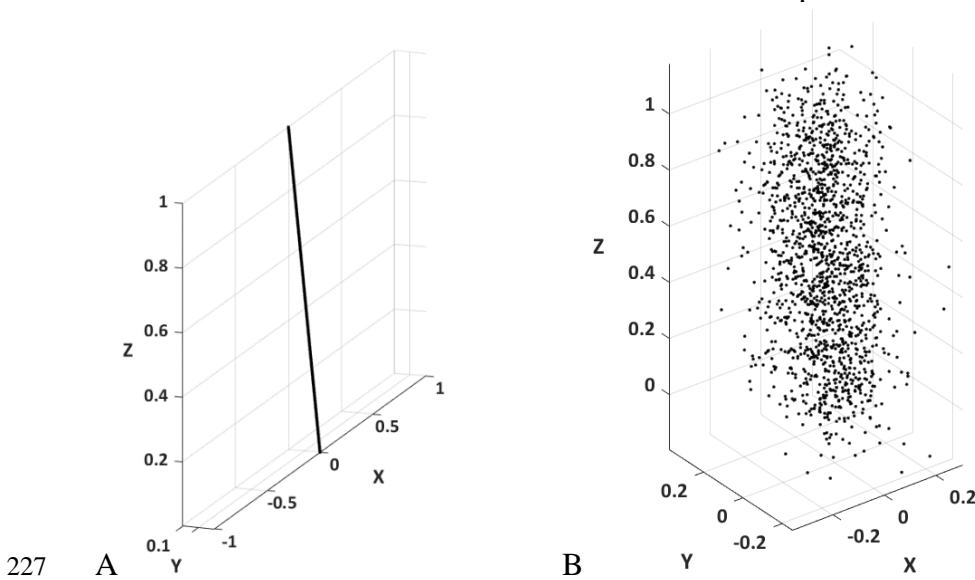
198 In a rock mass whose stress distribution has been disturbed by mining activity, a seismic
199 emission is mainly associated with slippage on rejuvenated faults and fractures as well as with
200 the formation of new fractures. The former constitute the main network of fractures while the
201 latter form the network of micro-fissures. Slippage and expansion of the main fracture network is

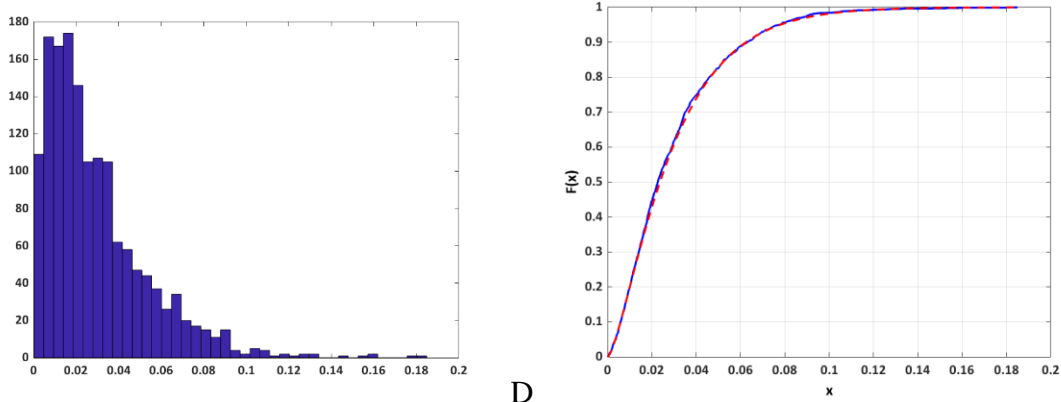
202 the source of some of the registered events spatially distributed along with systems with a
 203 relatively simple linear structure, e.g. planes or straight lines. The spatial distribution of other
 204 phenomena is more chaotic in character and greatly depends on the mineral composition and
 205 texture of the particular rock.

206 Every measurement involves some level of error. The location of emission sources is also
 207 erroneous, which causes perturbation of localized sources in relation to the actual positions of
 208 these sources and blurs the undisturbed image of the emission cloud. The purpose of collapsing
 209 is to limit at least partially such blurring and reduce perturbation. To this end, the sources are
 210 relocated and are shifted towards local emission densities.

211 The perturbation of the actual location of an emission source occurs randomly. This means that
 212 the total shift vector, i.e. the sum of three orthogonal vectors oriented in line with the directions
 213 of the individual axes of the coordinate system, is random. It can be assumed in this case that the
 214 components of the displacement along these three orthogonal directions have a normal
 215 distribution with individual mean values and dispersions. It can be argued that if each of these
 216 distributions is standardized, the total degree of displacement will be random in terms of
 217 direction and value defined by χ^2 distribution with three degrees of freedom (Evernden, 1969).
 218 Therefore, the closer two points are actually located, the greater the chance (in a statistical sense)
 219 that the distance between them as a result of perturbation will increase more in relation to the
 220 original distance than will the relative distance of points positioned further apart.

221 Let us consider the example presented in Figure 2, in which the location of real seismic sources,
 222 uniformly distributed on a straight line Figure 2A, has been affected by perturbation. These points
 223 are then dispersed in random directions at a random distance. Each of the X, Y and Z coordinates
 224 of the relocation vector is a random variable and has an identical normal distribution with a mean
 225 value of zero and a variance of 0.1. Figure 2B presents the points cloud modelled on this basis,
 226 which shows the distribution of emission sources after perturbation.





228 C
229

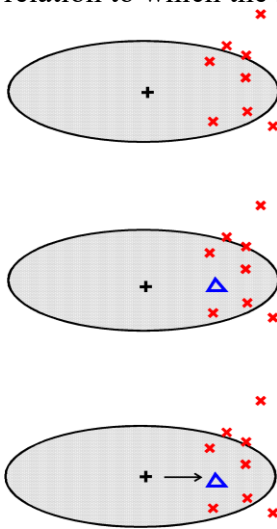
D

Figure 2. Population of points arranged on a straight line before A) and after B) perturbation of their positions. C) a histogram of the displacement vector length during the perturbation process, D) a comparison of the distribution function of the empirical distribution (red curve) and the theoretical distribution (blue curve) prepared for the needs of the Kolmogorov-Smirnov test.

234

235 Figure 2C presents an empirical histogram of the length of the displacement vector obtained
236 during perturbation. Because each vector coordinate of a perturbation is a random variable with
237 normal distribution, the square of the vector length of the perturbation, being the sum of the
238 squares of the vector coordinates of the perturbation with normal distribution, has χ^2 distribution
239 with three degrees of freedom. This becomes clear after performing the Kolmogorov-Smirnov
240 statistical test (K-S test). This test compares the empirical cumulative distribution function with
241 the theoretical cumulative distribution function of χ^2 distribution. Figure 2D presents both
242 cumulative distribution functions. The K-S test, in this case, shows the compatibility of both
243 kinds of distribution.

244 The collapsing procedure is designed to reduce the perturbation of emission source locations. It
245 involves gradually shifting emission sources towards local source densities. What is important to
246 note is that the relocation of each emission source takes place within its error ellipsoid, in
247 relation to which the source's location was established. The procedure is shown in Figure 3.



248

249 **Figure 3.** Image showing the relocation of seismic emission sources towards local emission
 250 source densities.

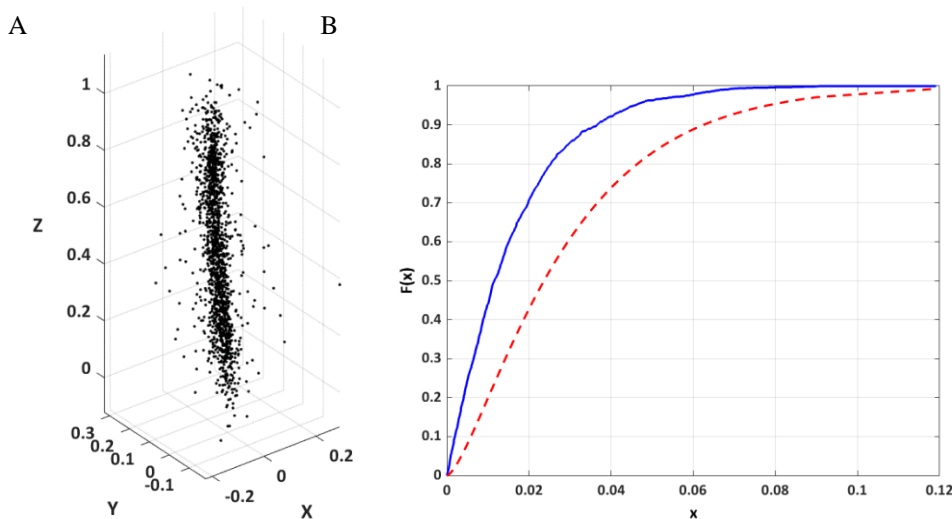
251

252 For each localized hypocenter:

- 253 • the localization error ellipsoid (black cross) is calculated for a given confidence interval as well
- 254 as all phenomena whose hypocenters lie within this ellipsoid
- 255 • the center of gravity is determined for the points within the error ellipsoid (blue triangle)
- 256 • the hypocenter of the analyzed phenomenon is shifted towards the center of gravity (the
- 257 ellipsoid remains in its original position)

258

259 In a particular iteration, positions from the previous iteration, which have not been updated in the
 260 current iteration, are taken into account as successive hypocentres are displaced. Shifted
 261 hypocentres create a new set of locations. The entire relocation procedure is repeated in the same
 262 way for each subsequent iterative step until the translation population assumes the form of a chi-
 263 square distribution with three degrees of freedom. The procedure is checked using the
 264 Kolmogorov-Smirnov test (K-S test) assessing the compliance of the empirical distribution with
 265 theoretical distribution χ^2 . As was mentioned above, in subsequent iteration cycles the error
 266 ellipsoids do not change their position.



267

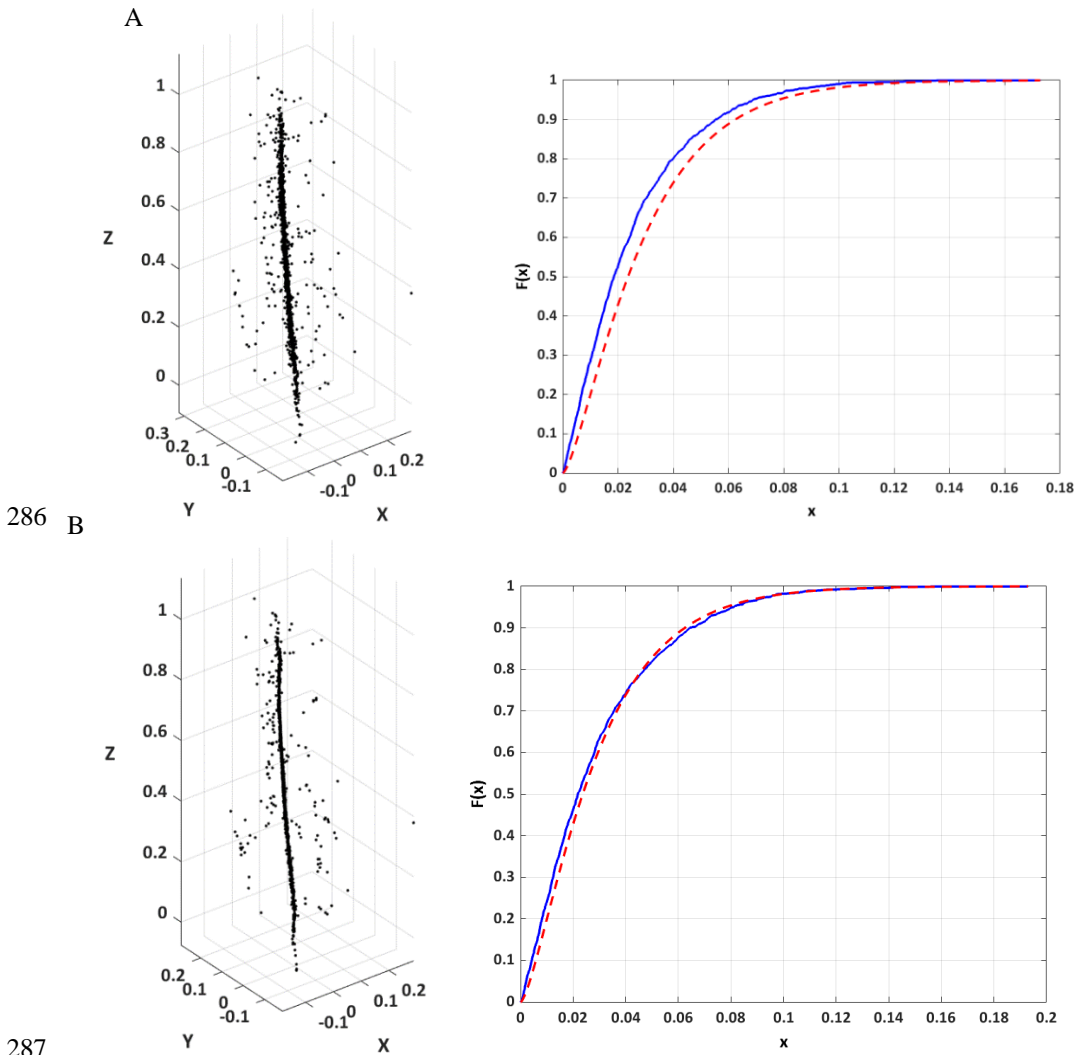
268

269 **Figure 4.** A) The population of points after the first stage of the relocation operation. B) A
 270 comparison of the empirical distribution function (red curve) with the theoretical distribution
 271 (blue curve) after the first collapsing step for the needs of the Kolmogorov-Smirnov test.

272

273 Figure 4 A) presents the points population after the first relocation step. As can be seen, the
 274 distance between points has been reduced. The empirical cumulative distribution of the
 275 relocation vectors in the first collapsing stage is represented in Figure 4B by a dashed red curve.
 276 It is compared in the Kolmogorov - Smirnov test with theoretical distribution. χ^2 . As can easily
 277 be seen, the two distribution functions are very different. Also, the K-S test result is negative. As
 278 has been noted above, if the hypothesis is rejected, the next relocation step is performed and the
 279 test is carried out once more. The procedure is repeated until the total distribution of
 280 displacement length achieves distribution χ^2 (thus adopting the hypothesis that both distributions
 281 are compatible) or when no progress is observed in matching both distributions in subsequent

282 iterations. In turn, Figure 5A and 5B show the distribution of sources after the second and
 283 relocation steps along with the empirical distributions of total displacements against the
 284 backdrop of theoretical distributions.
 285



289 **Figure 5.** The second A) and third (final) B) relocation stage. The left column presents the
 290 location of sources following relocation and the right column compares the empirical and
 291 theoretical cumulative distribution functions after each subsequent.
 292

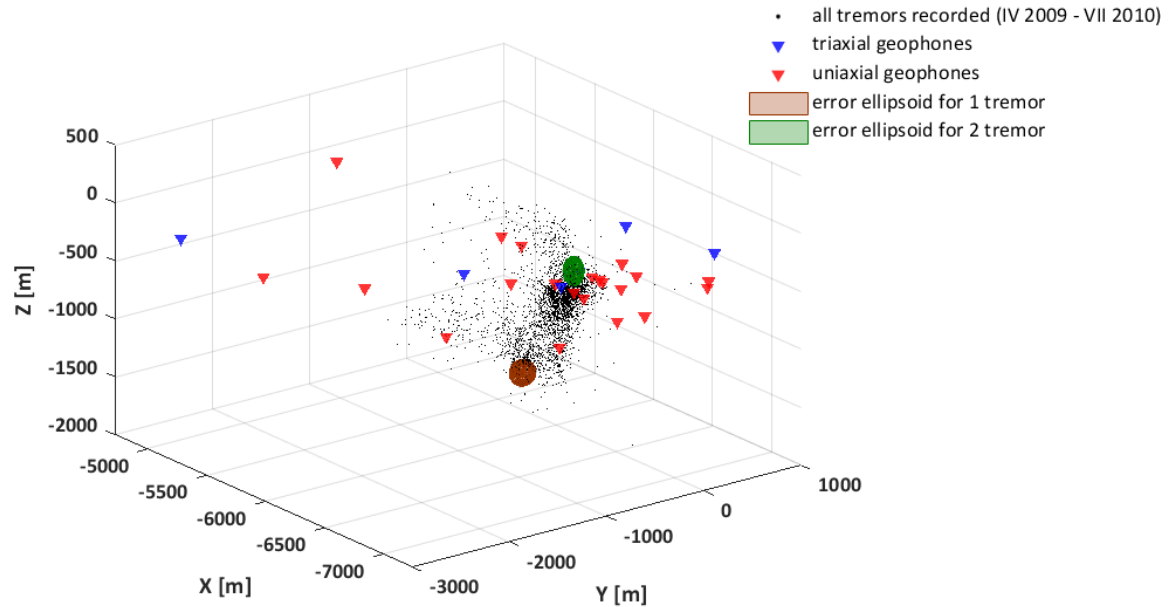
293 In the case of the example presented above, after the third step, most sources had already been
 294 relocated to a straight line, the location of which reflects the original location of the sources. It is
 295 also worth noting that not all the points were relocated. If for a given source the error ellipsoid
 296 with which it has been located is insufficient and does not include other sources, then the source
 297 is not relocated. The size of the ellipsoid is related to the adopted confidence level. In this case, it
 298 was assumed to be 0.95, which means that there is a 0.95 probability that the source is located
 299 within the error ellipsoid.
 300

301 **4 Data**

302 The Laboratory for Monitoring Mining-Induced Seismicity (LMMIS) conducted research on
303 local seismicity caused by underground coal mining in the Bobrek mine. These studies were part
304 of the IS-EPOS project(<https://tcs.ah-epos.eu/#episode:BOBREK>, accessed January 2020).
305 Within their framework, a total of 2995 tremors were recorded and located. They were registered
306 as a result of the exploitation of coalface 3/503 in the period between April 2009 and July 2010.
307 The hypocenters of these tremors occurred at various depths, ranging from 300 m below ground
308 level to more than 2300 m below ground level. The local magnitude of these events ranged
309 between 0 and 3.7. The most powerful tremor had a local magnitude $M_L = 3.7$ occurred on
310 December 16, 2009. This mining-induced tectonic event was associated with the local tectonic
311 structure of the Bytom Syncline(Kozłowska et al., 2016).

312 The Bobrek mine seismic network consists of 27 geophones with a recording band above 1 Hz. It
313 is composed of 21 uniaxial and 6 triaxial geophones, all with a sampling frequency of 500 Hz.
314 Most are located at the level of the exploited seam (approximately 750 m below the surface), two
315 at sea level and one at surface level. During the analyzed period, individual geophones were
316 serviced and repaired. As a consequence, only those geophones that were operational on the day
317 a particular event occurred were included in the location.

318 The locations were determined using the classical method for locating tremor sources based on
319 uniaxial (vertical) sensors and triaxial sensors according to the registration times of the first
320 seismic signal. An approximate model of medium velocity in the area of seam 503 was adopted,
321 for which the velocity of longitudinal wave propagation (used for localization) was 3850 m / s.
322 The location of geophones, along with the location of the sources of all registered seismic
323 tremors, is presented in Figure 6.



324

325 **Figure 6.** Seismic network of the Bobrek mine with tremors registered between April 2009 and
 326 July 2010. Uniaxial geophones are marked with red triangles and triaxial geophones with blue
 327 triangles.

328

329 Figure 7 features a histogram showing the seismic activity for each month. This histogram
 330 indicates that seismic activity changed during the period in which the mine was in operation.
 331 From December 2009 to May 2010, the number of tremors increased significantly, especially
 332 when compared to the months preceding this increase. This coincided with the moment when the
 333 active coalface crossed the Bytom basin axis.

334 The same figure shows the percentage of seismic phenomena whose sources were located below
 335 seam No. 503 in relation to the total number of such events. Face 3 of this seam lies at a depth of
 336 approximately 700 m below the surface and, as such, the majority of the tremors were generated
 337 below this depth and only a small (roughly 10%) number occurred above. The number of
 338 tremors below the seam was calculated by taking into account the depth of the coalface at the
 339 end of each period. Most of the tremors occurred below seam 503. During this period, a small
 340 number of tremors were also recorded in the seam roof.

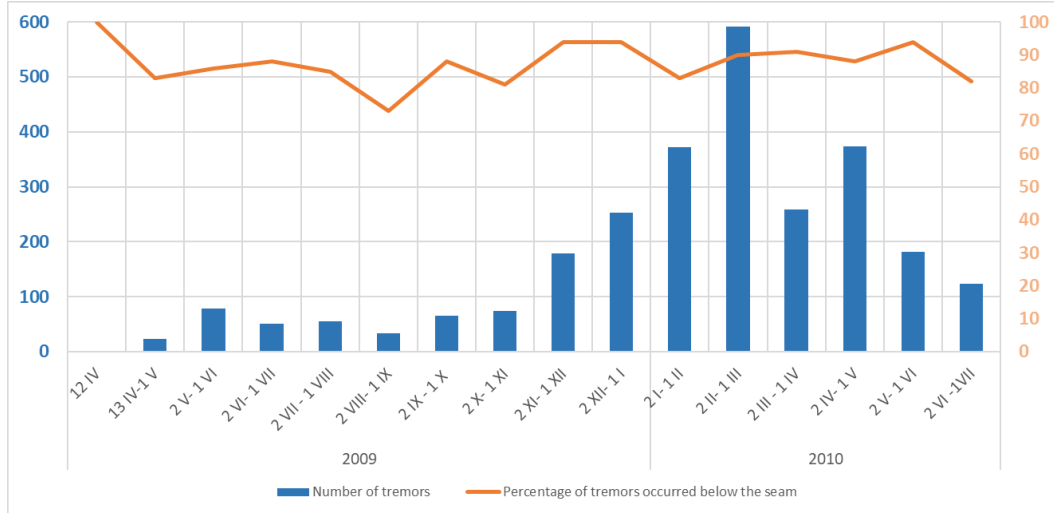


Figure 7. Number of tremors for each month between April 2009 and July 2010

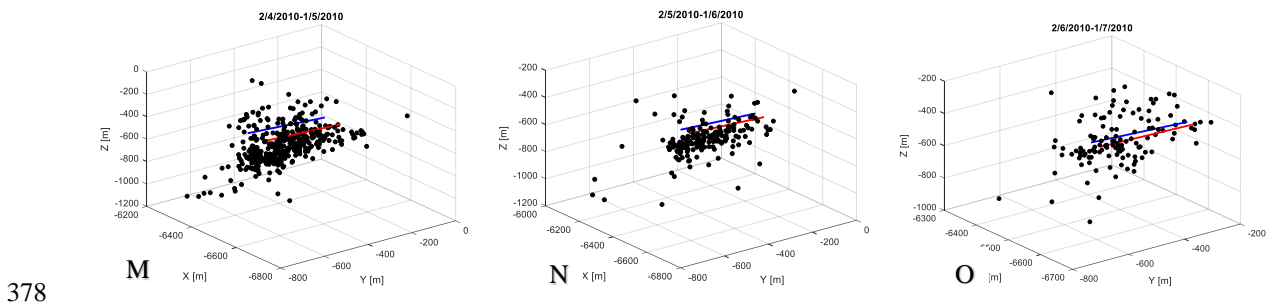
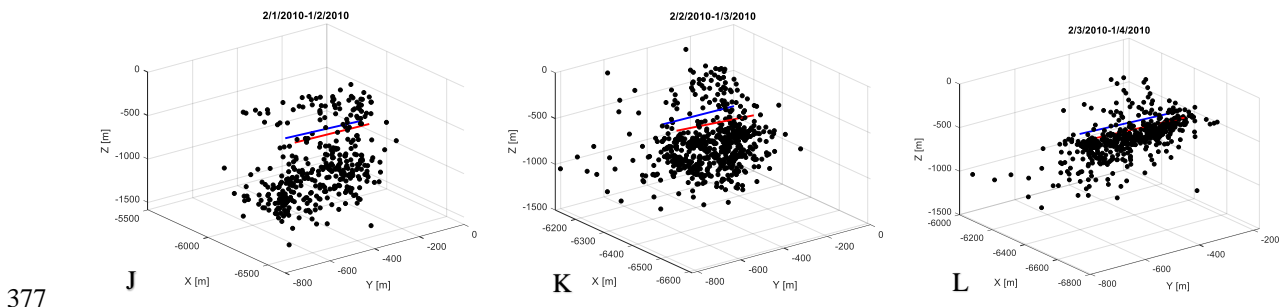
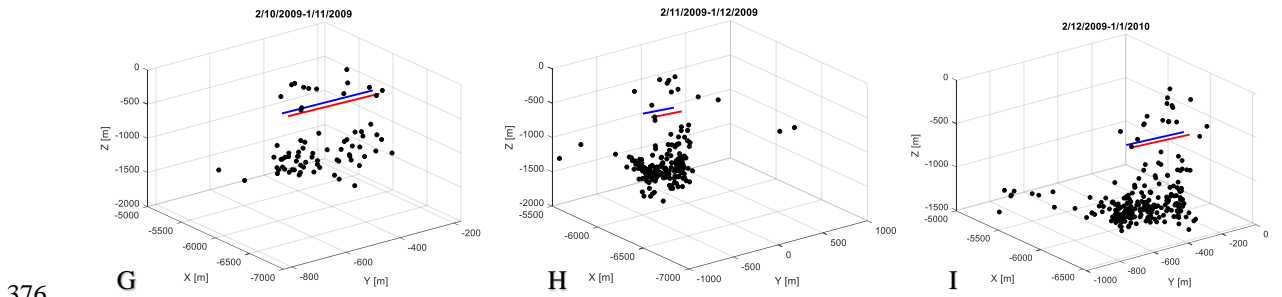
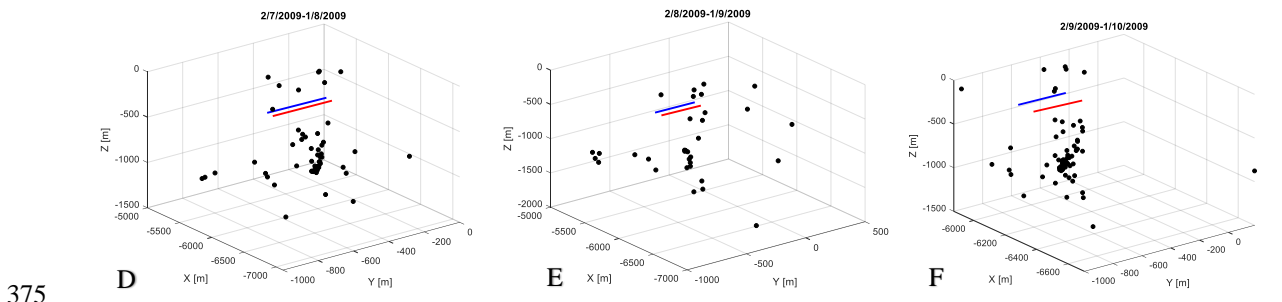
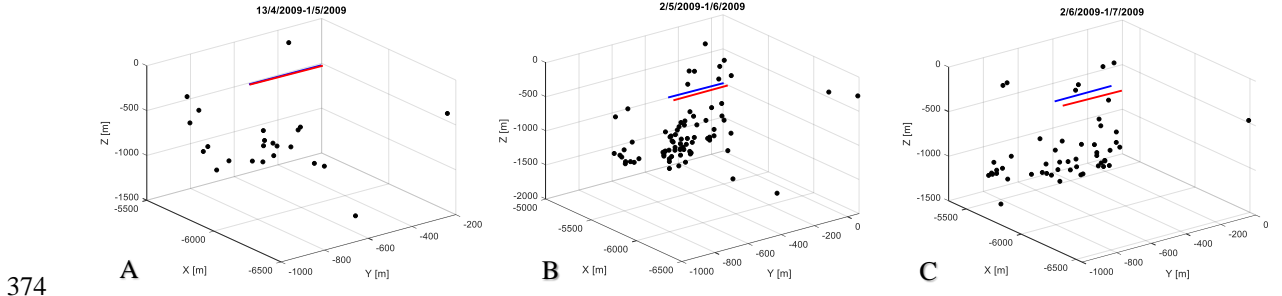
As has already been noted (Marcak and Mutke, 2013) the highest energy tremors took place 300-800 m below the mining level and were located at a short distance from the axis of the Bytom Basin.

The key to implementing the collapsing procedure is determining the location ellipsoid error for a seismic event. The orientation of the error ellipsoid is determined by the spatial configuration of the sensors in relation to the source location. The size of the ellipsoid is established by the partial errors in the measured parameters. To determine the error ellipsoid, it was assumed that the error in the time of the P wave was, depending on the signal quality, 4 ms. However, greater accuracy was achieved with good quality signals, dropping to as low as 2 ms. The sensor location error parameter was estimated at 0.1m. In addition to the two types of error mentioned above, the magnitude of the location error is also affected by the simplified velocity model for the center of seismic wave propagation, both in terms of the inaccuracy of the geometric structure and the variable speed values. Assuming that the errors are random with normal distribution and that the measurement is not burdened with a permanent error caused by, for example, defective measuring equipment or significant differences in conditions around the ellipsoid sensors, the location of an emission source can be defined as follows (Jones and Stewart, 1997; Leśniak, 2015):

$$\sigma_s^2 = \sigma^2 (G_s^T G_s)^{-1} \chi_3^2(\alpha) \quad (1)$$

where G_s is a matrix containing partial derivatives of spatial residues, σ^2 constitutes the variance of the data while $\chi_3^2(\alpha)$ is the chi square distribution value with three degrees of freedom for significance level α (in our case 99.5%). Sample error ellipsoids for the location of the foci of two tremors occurring at different depths at the adopted significance level are shown in Figure 6. The distribution of the tremor cloud is shown in monthly time intervals - before and after collapsing, together with the current position of the active coalface in Figure 8 A) - O) and Figure 10 A) - O). The coalface progressed at an average pace of 50 m from month to month. In each sketch, the blue line indicates the position of the coalface at the beginning of the selected

370 time interval, and the red line the position at the end. The mining works proceeded from north to
 371 south perpendicular to the axis of the Bytom basin. The axis of the Bytom basin was crossed in
 372 April 2010, two months before mining of the seam came to an end.
 373



379 **Figure 8.** A-O Location of the point cloud in monthly intervals along with the current position of
380 the coalface at the beginning and end of the interval

381
382 It can easily be seen that in the early months of mining activity, seismic emissions were
383 relatively low and occurred mainly between 500 and 1000 meters below the seam. In the next six
384 months of mining at the seam, the emissions were similar to one another in terms of both
385 intensity and the average depth of the source location. Starting from September 2009, there was a
386 significant increase in emission intensity as well as a gradual decrease in the location depth of
387 the sources. In the last two months of mining activity (sketches 8N and 8O), emissions occurred
388 relatively close to the seam, where coal was being mined.

389

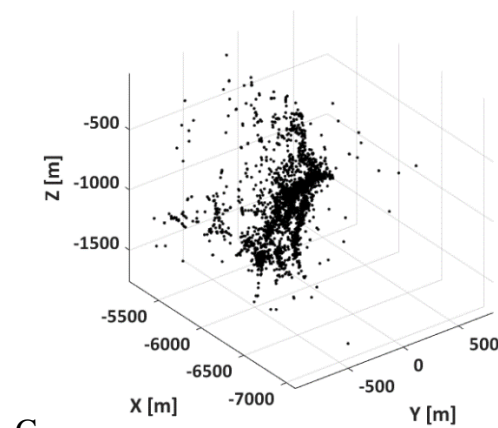
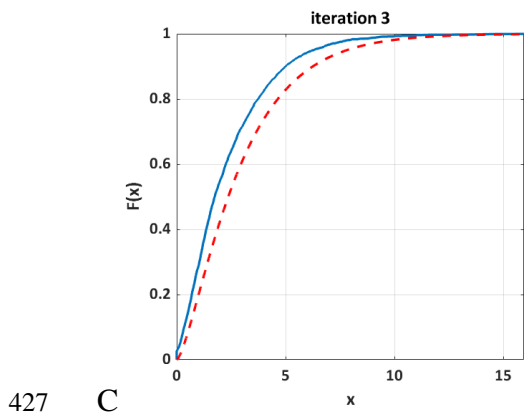
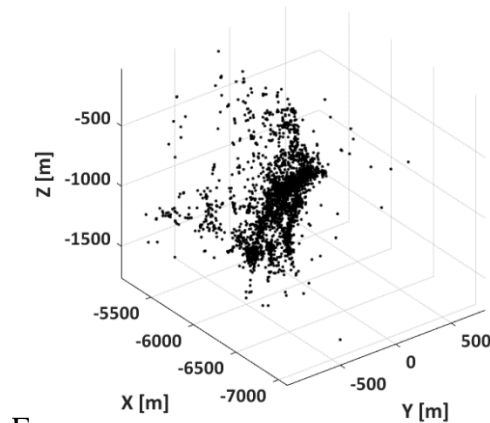
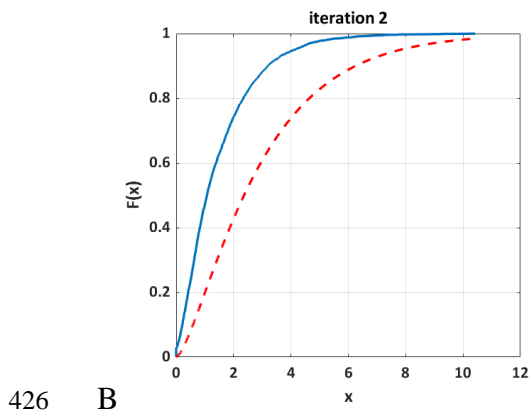
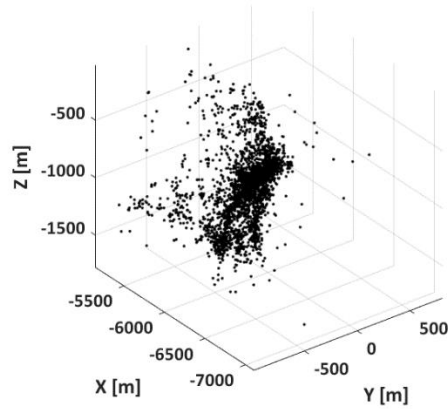
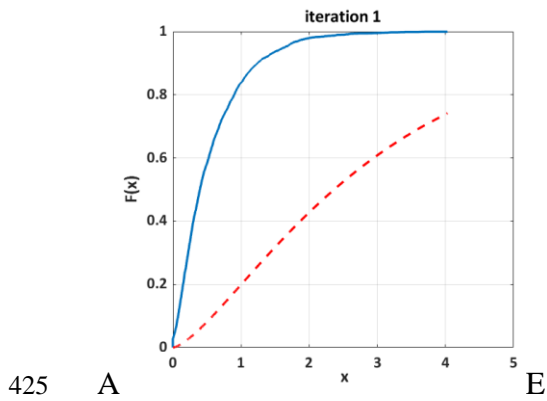
390 **5 Results**

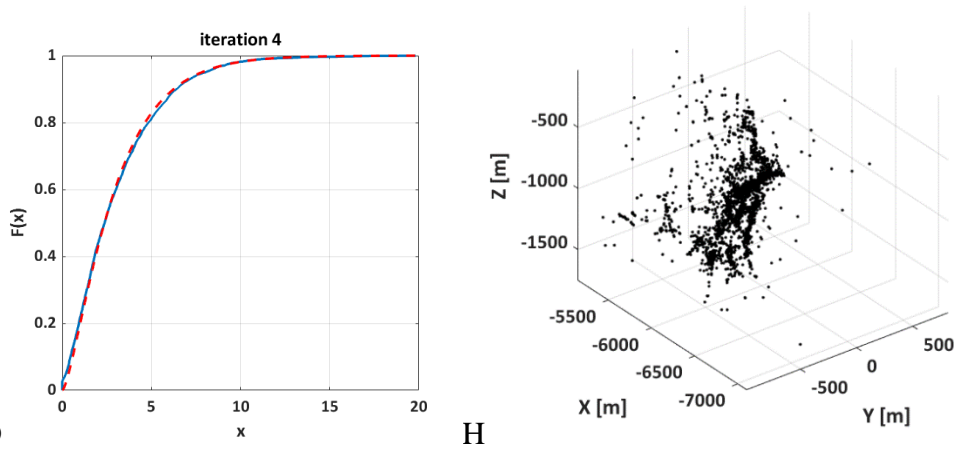
391 All the foci of seismic emissions recorded during the analyzed time period underwent relocation
392 procedure. As was described in section 3, an error ellipsoid was calculated for each source within
393 which displacement towards a local density center was possible. The process was iterative in
394 form, testing through repetition whether all displacements form a χ^2 distribution. As was
395 mentioned above, the key to the relocation process is the size and orientation of the error
396 ellipsoid. The orientation mainly depends on the spatial configuration of the seismic network and
397 its size, in accordance with formula 1, as well as on the variance of the data and the confidence
398 level used for the cut-off. A high degree of location accuracy (a relatively small error ellipsoid)
399 does not allow for any significant displacement of localized sources. A lower degree of location
400 accuracy (larger error ellipsoid) allows for larger displacements. The creators of the method
401 suggest using relatively large values for the ellipsoid confidence level, arguing that a change
402 from 2σ (95%) through 3σ (98%) up to 4σ (99.86%) does not significantly affect the collapsing
403 results (Jones and Stewart, 1997). In turn, the data variance should be estimated on each occasion,
404 as was discussed in the previous section.

405 First, the results of the collapsing procedure for the entire data set were presented. The location
406 of the tremors in each iteration is shown in sketches 9 E-H. The compatibility of the theoretical
407 and empirical distributions was checked using the Kolmogorov-Smirnov test in each iteration.
408 The differences between theoretical and empirical distributions are presented in sketches 9 A-D.
409 One can be observed that in subsequent stages the difference between the theoretical and
410 empirical cumulative distribution function decreases. The procedure is carried out until the null
411 hypothesis is achieved, i.e. when both distributions are compatible with each other. The size of
412 the ellipsoid used for the calculations is 0.995. The statistical significance value (parameter p)
413 was examined. In the first relocation step it was 0, and in the following steps: $6.7507e-263$,
414 $5.0692e-44$, 0.0062. In the 4 iterations, distribution compatibility was achieved within the
415 assumed error.

416 Sketches 10 A-O show the post-relocation tremors registered in individual months of mining
417 activity. A comparison of this data with the distribution of tremors before the collapse (sketches
418 8 A-O) shows that the number of sources involved in relocation increases as the active coal face

419 approaches the axis of the Bytom basin. This process can be observed by comparing the point
 420 cloud images for individual months in Figures 8 and 10 beginning from Sketches H to O. Here
 421 we can observe the collapse of the cloud into one-dimensional linear structures. These structures
 422 can generally be divided into two groups. The first comprises horizontal structures closer to the
 423 seam running parallel to the active coalface (e.g. sketches 10 L, M, N). The second consists of
 424 structures with an almost vertical course and located at a greater depth (as in sketches 10 E, H, I).





428

D

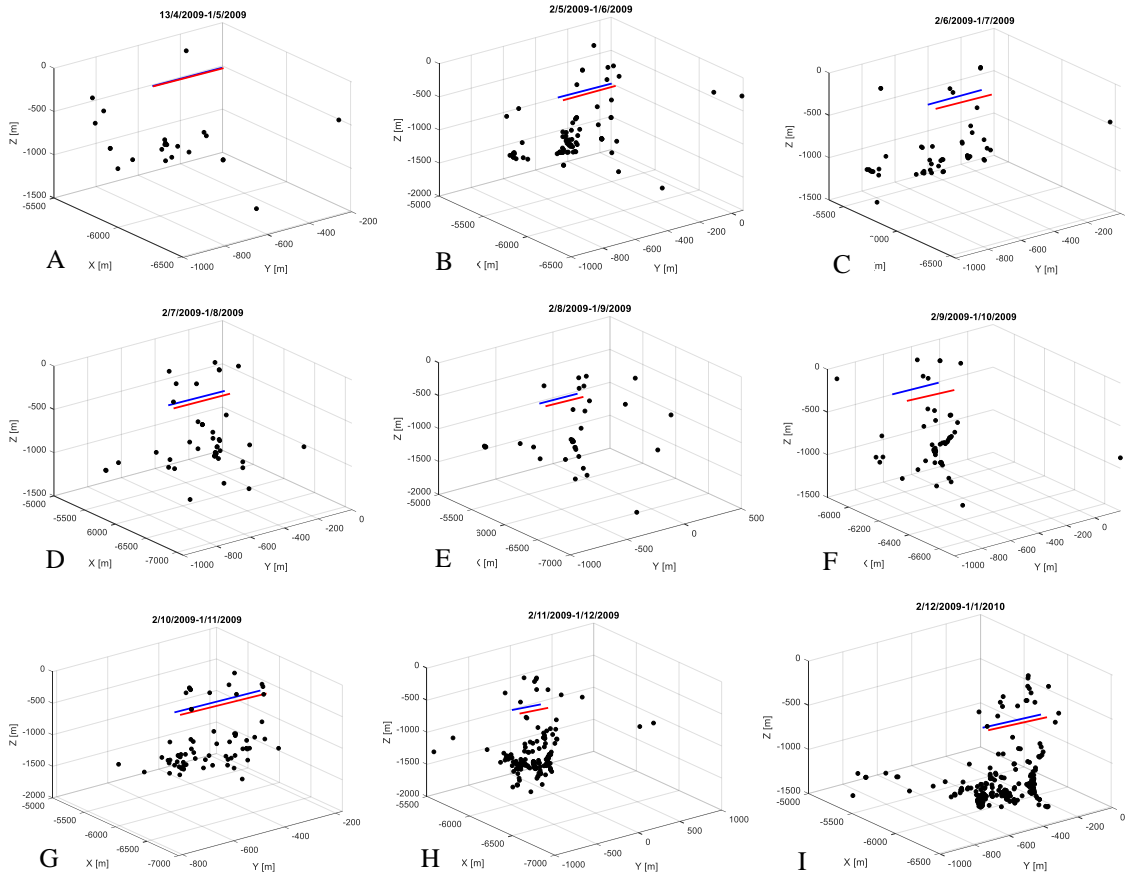
H

429

430 **Figure 9.** A) - D) A comparison of theoretical and empirical distribution functions. The red
 431 dashed curve denotes the empirical distribution function while the blue dashed curve represents
 432 the theoretical distribution function. E) -H) locations of tremor cloud foci in subsequent
 433 iterations

434

435



436

A

B

C

437

D

E

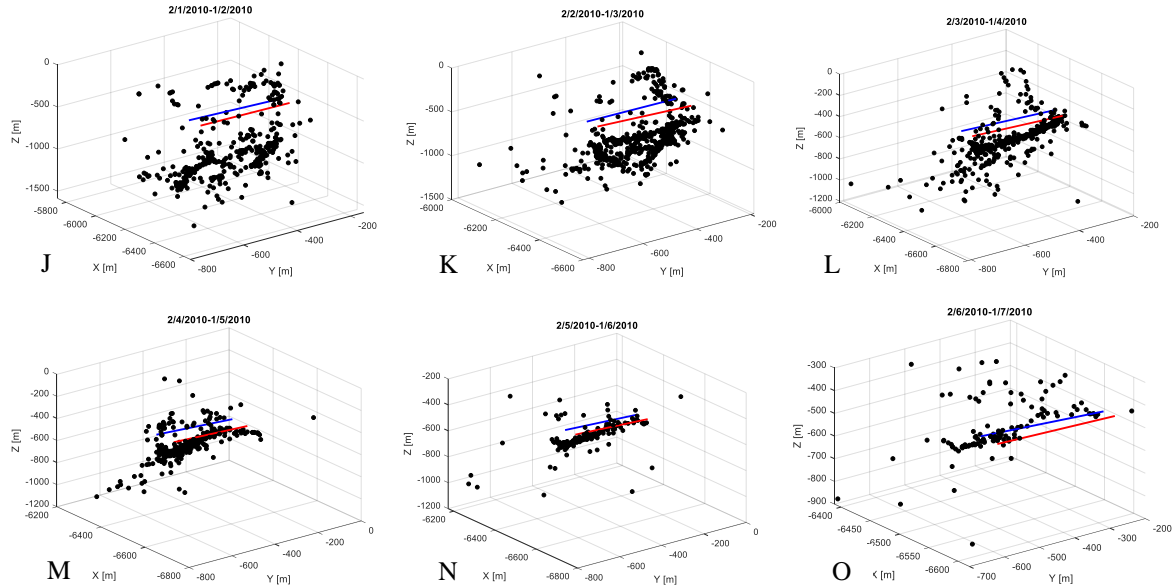
F

438

G

H

I

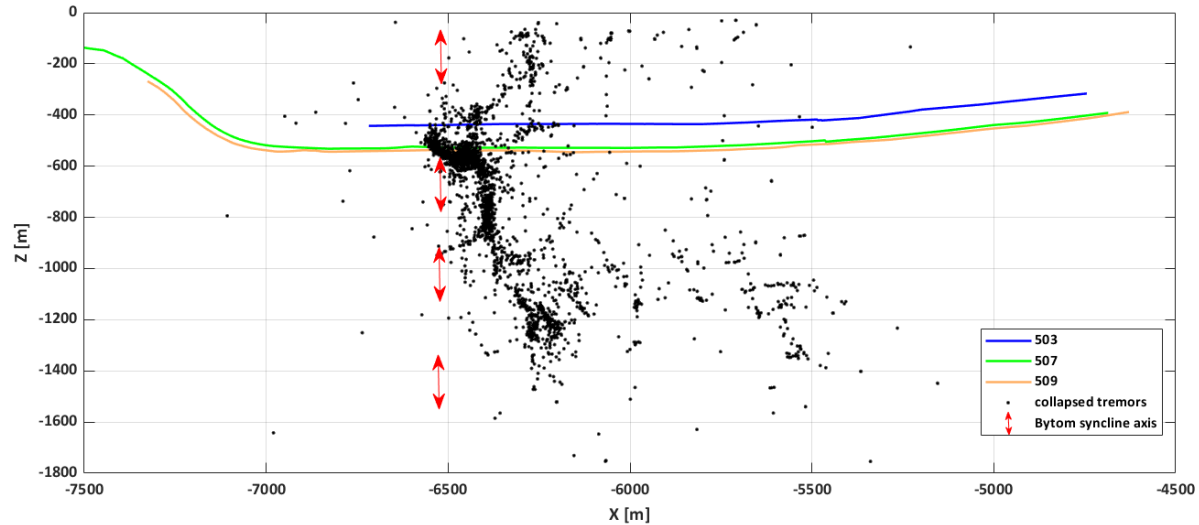


439

440

441 **Figure 10.** A) - O) Location of displaced point cloud via the collapsing method in monthly
 442 intervals along with the current position of the active coalface at the beginning and end of the
 443 interval.

444 Figure 11 shows the emission cloud following relocation set against the background of both
 445 seam 503 and two deeper, previously mined seams 507 and 509. Following the collapse of the
 446 sources, most phenomena were concentrated below the seam where mining activity was taking
 447 place (blue line) in the vicinity of the previously mined seams (lines green and orange). A
 448 specific image is likewise formed by the foci of numerous tremors grouped in narrow zones with
 449 a vertical or almost vertical course. They occur near the axis of the Bytom basin, the course of
 450 which is marked with red arrows. A relatively small number of tremors occurred above seam
 451 503. One important trend to note is the sharp drop in the number of tremors that occurred once
 452 the basin axis was crossed, first above the seam and then below it.

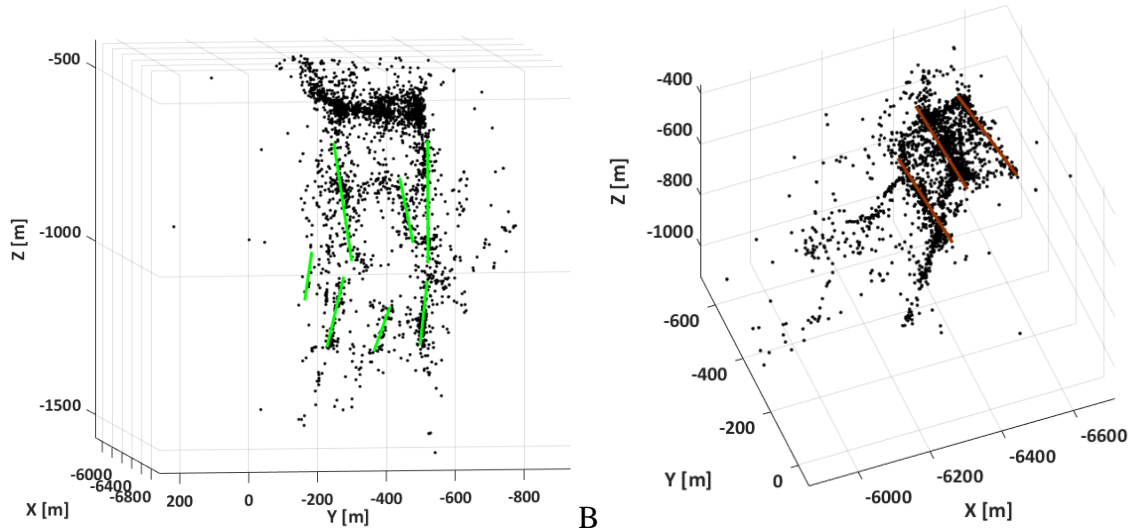


453
 454 **Figure 11.** Vertical cross-section of seam 503 and previously mined seams 507 and 509 located
 455 below along with the location of emission sources after relocation as well as the axis of the
 456 Bytom basin.

457
 458 Generally speaking, following relocation the cloud representing the foci of tremors is more
 459 heterogeneous, as is manifested in the occurrence of local densities of various shapes. Most often
 460 they assume a shape similar to straight lines and planes with different orientations.

461 **6. Interpretation**

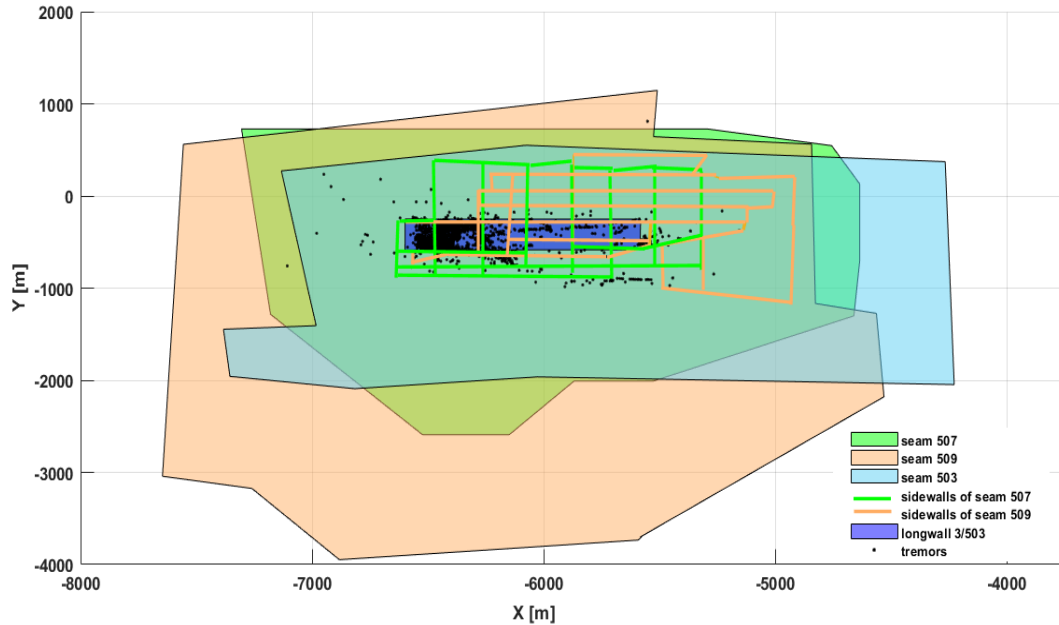
462 Based on the results presented above, an attempt was made to identify linear structures using a
 463 cloud of seismic tremors displaced by means of the collapsing method in the data set taken from
 464 the entire period of mining activity (Figure 12 A-B). The structures were identified with Matlab
 465 software, whose graphic interface allows for a 3D visualization of a cloud, rotation, and scaling.
 466 The goal was to identify distinct groups arranged along straight lines or on planes. Small
 467 structures were not marked, including those that were small in size and those containing a small
 468 number of points. This is because their location would have been largely subjective.



469 A B
 470
 471 **Figure 12.** Separated structures A) vertical and B) horizontal in the cloud after collapsing
 472

473 The separated structures are associated with areas characterized by a rectilinear course with an
 474 above-average density of events. They are associated with real places of intensive seismic
 475 emission that run along fracture zones with weakened rock mass. Green lines with an almost
 476 vertical course can be interpreted as local tectonic discontinuities that have been activated as a
 477 result of mining activity. Their occurrence was previously postulated by Marcak and
 478 Mutke(2013) and was associated with the occurrence of flexures (monoclinial fold) in the Bytom
 479 basin. In basins of this type, we can expect the occurrence of fracture systems of varying scale
 480 with an almost vertical course and thus perpendicular to the axis of the basin and the selected
 481 seam(Li et al., 2018).The structures shown in Figure12 are characterized by a depth of
 482 occurrence of between 500 m and 1400 m ppm, i.e. they are located below the two exhausted
 483 seams.

484 The brown lines with a more or less horizontal direction run parallel to the active coalface and
 485 progress in tandem with its progress. Significantly, they occur deeper than exploited seam 503,
 486 namely in the immediate vicinity of exhausted seams 507 and 509. Figure 13 presents, against
 487 the backdrop of seams 503, 507 and 509, the location of the collapse cloud and the range of
 488 exploited face 3/503 as well as the location of the shafts delimiting the exploited faces of seams
 489 507 and 509.



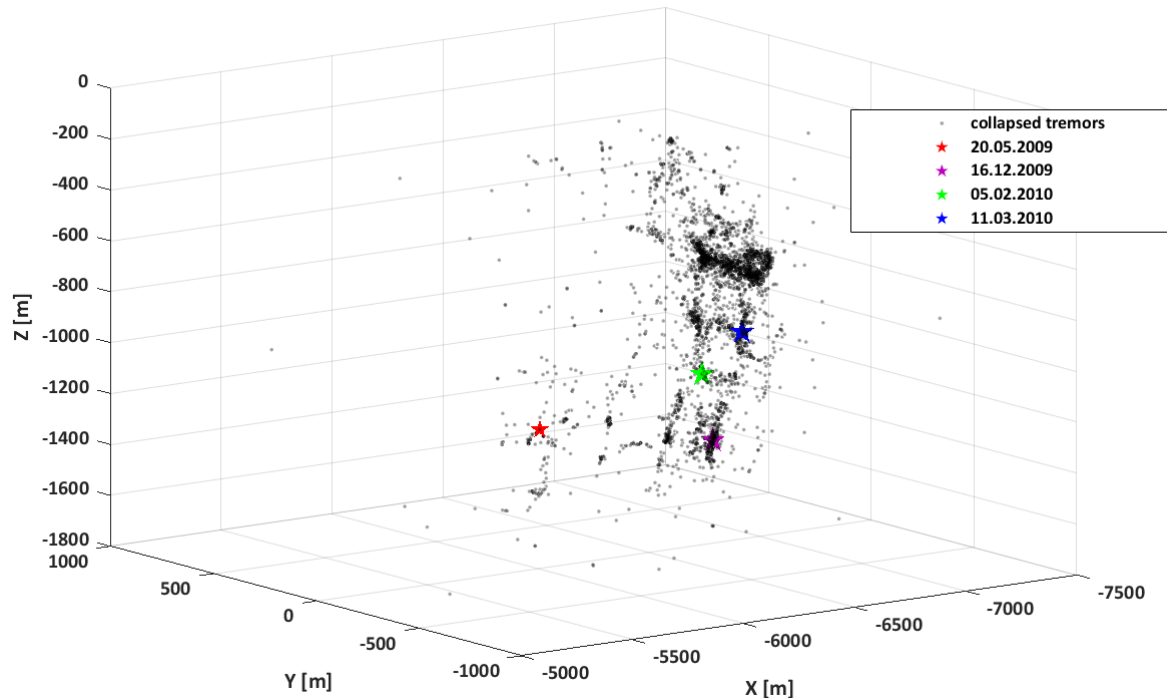
490

491 **Figure 13.** Flat projection of the boundaries of seams 503, 507 and 509, the range of exploited
 492 face 3/503 and the location of the shafts delimiting the exploited faces in seams 507 and 509.
 493 The black points show the location of the cloud of phenomena the following collapse.

494

495 The shafts of exploited seams (lines marked in green and orange) roughly demarcate the zones
 496 located below exploited seam 3/503, where the continuity of the rock mass was disturbed as a
 497 result of mining activity prior to the exploitation of seam 503. These disturbed zones were the
 498 site of an intensive seismic emission faithfully depicted by the spatial distribution of seismic
 499 emission sources (see Figure 13). The horizontal structures marked with brown lines in the cloud
 500 of phenomena in Figure 12 have similar positions and spatial orientations to the shafts of earlier
 501 exploited seams 507 and 509. Such compliance is very good for structures closer to seam 509.

502 As has already been noted in the case of mining-induced emissions, two types of seismic tremors
 503 are generally distinguished— mining-induced tremors and tremors of mining-tectonic origin (Stec,
 504 2007). Mining and tectonic seismicity are caused by the interaction between, on the one hand,
 505 mining activity, both current and in the past, and, on the other, locally existing seismogenic
 506 zones such as faults as well as areas affected by mining activity. Mining seismicity is associated
 507 with events located near active mining excavations. The vertical structures isolated from the
 508 emission cloud were linked above with relatively large fracture zones, which in turn are
 509 connected with the flexure of the Bytom basin. These structures include three of the four tremors
 510 with energy greater than 10^7 J registered during mining of face 3/503 (see Figure 14).



511
 512 **Figure 14.** Location of the foci of the four largest tremors recorded during mining of the seam
 513 against the backdrop of the emission cloud following relocation.

514
 515 These tremors are located at relatively great depths, which indicates that they are of mining-
 516 tectonic origin rather than being induced by mining activity alone. They form part of the linear
 517 structures in the emission cloud isolated in Figure 12, which are located below the shafts
 518 surrounding the faces of seams that have been mined.

519 The above observations suggest that vertical or nearly vertical linear structures identified after
 520 collapsing the cloud of phenomena correspond to actual zones of rock mass discontinuity
 521 activated during mining. The emission recorded during the mining of face 3/503 activated these
 522 faults, leading to a series of numerous tremors with energy emitted over a wide range. In turn,
 523 horizontal linear structures located near the exploited seams correspond to the rock mass zones
 524 directly affected by the mining of hard coal deposits in the region of the Bytom basin axis.
 525 Deeper horizontal structures, which have also been activated by mining and, like vertical
 526 structures, occur near the basin axis, may be associated with discontinuities and stress
 527 distribution in the synclinal region, as is mentioned by Marcak and Mutke(2013).

528 7. Summary

529 The relocation method allows for greater accuracy in identifying the structures associated with
 530 seismic zones in the cloud of seismic emission sources. According to the authors of the method,
 531 the source cloud after relocation corresponds, statistically speaking, to the original cloud before
 532 relocation, in the sense that it provides a picture of the spatial distribution of sources acceptable
 533 within the framework of location error. Both distributions clearly differ in their degree of

534 heterogeneity. After the collapse, this heterogeneity increases significantly and, as a rule, there is
535 a clear tendency towards a concentration within the cloud. They are identified with seismically
536 active zones such as systems of fractures and fissures, faults and areas affected, e.g. by mining
537 activity. Because seismogenic zones are often associated with areas of high stress concentration,
538 collapsing makes it possible to verify certain hypotheses regarding the distribution of tectonic
539 stress in a deformed rock mass.

540 Imaging of structures based on non-localized locations is in many cases a subjective operation
541 that does not guarantee reproducible results. The collapsing operation makes it possible to reduce
542 the degree of subjectivity when identifying structures and as a consequence increase the
543 reliability of the method itself.

544 It is important to note that the more numerous the set of registered phenomena and the greater
545 the seismic activity the more effective this method is. In the case of seismic emissions registered
546 in underground mines, the main triggering factor is mining of the deposits. The site where these
547 deposits are mined gradually moves in accordance with the established mining plan. The method
548 described in this article makes a positive result possible if the zones of each seismogenic zone
549 are imaged via at least several dozen phenomena.

550 Another factor that is key to its success is that it accurately determines ellipsoidal errors of
551 location for individual phenomena. If the location error is very small and the emission is likewise
552 small, the relocation of the sources will be small and the resolution of the point cloud will not
553 improve significantly. In turn, large error ellipsoids, which will overlap to a large extent, which
554 in turn will result in extreme cases in the sources collapsing too intensively into one or a few
555 centers containing most points. As is shown in practice, the best results are achieved when the
556 ellipsoid size is assumed at a confidence level of 99.5%.

557 The method discussed in this article ensures greater precision when mapping seismogenic zones
558 in a rock mass. As the example presented in this article shows, if used properly, the method
559 allows these zones to be connected with stress concentration sites as well as discontinuities and
560 damaged zones. Compared with other geophysical methods for mapping discontinuities and
561 monitoring dynamic changes in underground mines, seismology supported by appropriately
562 selected processing methods (as shown above) ensures the widest range and satisfactory
563 resolution.

564

565 **Data**

566 Dataset used for this research are available in IS-EPOS project(<https://tcs.ah-epos.eu/#episode:BOBREK>).

568 **References**

569 Asanuma, H., Ishimoto, M., Jones, R.H., Phillips, W.S., Niitsuma, H. (2001). A Variation of the
570 Collapsing Method to Delineate Structures Inside a Microseismic Cloud. *Bulletin of the*
571 *Seismological Society of America*, 91(1), 154-160, <http://dx.doi.org/10.1785/0120000063>

- 572 Asanuma, H., Kumano, Y., Izumi, T., Soma, N., Niitsuma, H., Baria, R. (2005). *Monitoring of*
573 *Reservoir Behavior at Soultz HDR Field by Super-Resolution Microseismic Mapping*. Paper
574 presented at Proceedings World Geothermal Congress, Antalya, Turkey.
- 575 Asanuma, H., Kumano, Y., Niitsuma, H., Wyborn, D., Schanz, U., Haring, M. (2008). *Current*
576 *Status of Microseismic Monitoring Techniques for the Stimulation of HDR/HFR Reservoirs*.
577 Paper presented at Australian Geothermal Energy Conference, Melbourne, Australia.
- 578 Evernden, J.F. (1969). Precision of epicenters obtained by small numbers of world-wide stations.
579 *Bulletin of the Seismological Society of America*, 59(3), 1365-1398.
- 580 Fehler, M., House, L., Scott Phillips, W. (1997). Identifying Structures in Clouds of Induced
581 Microseismic Events. *Society of Exploration Geophysicists*.
- 582 Geiger, L. (1912). Probability method for the determination of earthquake epicenters from the
583 arrival time only. *Bull St Louis Univ* 8, 60–71.
- 584 Gibowicz, J.S., Kijko, A. (1994). *An Introduction to Mining Seismology*. San Diego: Elsevier
585 Science.
- 586 Goszcz, A. (1999). *Elementy mechaniki skał oraz tąpnięcia w polskich kopalniach węgla i miedzi*.
587 Kraków: Wydawnictwo Instytutu Gospodarki Surowcami Mineralnymi i Energią PAN.
- 588 Havskov, J., Ottemoller, L. (2010). *Routine Data Processing in Earthquake Seismology: With*
589 *Sample Data, Exercises and Software*. Springer
- 590 IS EPOS (2017), Episode: BOBREK, <https://tcs.ah-epos.eu/#episode:BOBREK>,
591 doi:10.25171/InstGeoph_PAS_ISEPOS-2017-003
- 592 Jones, R.H., Stewart, R.C. (1997). A method for determining significant structures in a cloud of
593 earthquakes. *Journal of Geophysical Research: Solid Earth*, 102(B4), 8245–8254.
594 <https://doi.org/10.1029/96jb03739>
- 595 Kozłowska, M., Orlecka-Sikora, B., Rudziński, Ł., Cielesta, S., Mutke, G. (2016). Atypical
596 evolution of seismicity patterns resulting from the coupled natural, human-induced and
597 coseismic stresses in a longwall coal mining environment. *International Journal of Rock*
598 *Mechanics and Mining Sciences*, 86, 5–15. <https://doi.org/10.1016/j.ijrmms.2016.03.024>
- 599 Leśniak, A. (2015). Seismic network configuration by reduction of seismic source location
600 errors. *International Journal of Rock Mechanics and Mining Sciences*, 80, 118-128.
601 <https://doi.org/10.1016/j.ijrmms.2015.09.013>
- 602 Leśniak, A., Pszczoła, G. (2008). Combined mine tremors source location and error evaluation in
603 the Lubin Copper Mine (Poland). *Tectonophysics*, 456, 16–27.
604 <https://doi.org/10.1016/j.tecto.2007.04.012>
- 605 Li, Y., Hou, G., Hari, K.R., Neng, Y., Lei, G., Tang, Y., Zhou, L., Sun, S., Zheng, C. (2018). The
606 model of fracture development in the faulted folds: The role of folding and faulting. *Marine*
607 *and Petroleum Geology*, 89, 243–251. <https://doi.org/10.1016/j.marpetgeo.2017.05.025>
- 608 Marcak, H., Mutke, G. (2013). Seismic activation of tectonic stresses by mining. *Journal of*
609 *Seismology*, 17, 1139–1148. <https://doi.org/10.1007/s10950-013-9382-3>
- 610 McGarr, A. (2000). Energy budgets of mining-induced earthquakes and their interactions with
611 nearby stopes. *International Journal of Rock Mechanics and Mining Sciences*, 37, 437-443.
612 [https://doi.org/10.1016/s1365-1609\(99\)00118-5](https://doi.org/10.1016/s1365-1609(99)00118-5)
- 613 Mosegaard, K., Sambridge, M. (2002). Monte Carlo analysis of inverse problems. *Inverse*
614 *Problems*, 18, R29-R54. <https://doi.org/10.1088/0266-5611/18/3/201>
- 615 Phillips, W.S., House, L.S., Fehler, M.C. (1997). Detailed joint structure in geothermal reservoir
616 from studies of induced microearthquake clusters. *Journal of Geophysical Research*, 102(B6),
617 11,745-11,763. <https://doi.org/10.1029/97JB00762>

- 618
619 Rudziński, L., Dębski, W. (2013), Extending the double difference location technique-improving
620 hypocenter depth determination. *Journal of Seismology* 17, 83–94.
621 <https://doi.org/10.1007/s10950-012-9322-7>
622 Stec, K. (2009). *Characteristics of the processes taking place at the sources of high energy*
623 *tremors occurring in the Upper Silesian Coal Basin in Poland – regional character*. Paper
624 presented at 7th International Symposium on Rockbursts and Seismicity in Mines, Dalian,
625 China.
626 Stec, K. (2007). Characteristics of seismic activity of the Upper Silesian Coal Basin in Poland.
627 *Geophysical Journal International* 168, 757–768. [https://doi.org/10.1111/j.1365-](https://doi.org/10.1111/j.1365-246X.2006.03227.x)
628 [246X.2006.03227.x](https://doi.org/10.1111/j.1365-246X.2006.03227.x)